Delft University of Technology

Influence of Installation Method on the Axial Capacity of Piles in Very Dense Sand

Duffy, Kevin; Gavin, Kenneth; Korff, Mandy; de Lange, Dirk; Roubos, Alfred

Important note
To cite this publication, please use the final published version (if applicable).
Please check the document version above.

Influence of Installation Method on the Axial Capacity of Piles in Very Dense Sand

Kevin Duffy[1]; Ken Gavin[2]; Mandy Korff[3]; Dirk de Lange[4]; and Alfred Roubos[5]

Abstract: Three driven precast, four driven cast-in-situ, and four screw injection piles were installed and tested in dense to very dense sand at a site in the Netherlands. Each pile was instrumented with two types of fiber optic sensors and tested under axial compression. Through these tests, a comparison could be made of how different installation methods influence the pile base and shaft response. For example, large residual base stresses were measured in the driven precast piles after installation. Of the three pile types tested, the driven precast piles also reached the highest base stresses, mobilizing their full base resistance at comparatively low displacements. The base response of the driven cast-in-situ piles was also like that of a driven precast pile with residual stresses excluded. In contrast, the screw injection piles mobilized much lower ultimate base resistances and with a much lower stiffness. In terms of shaft resistance, the precast piles showed friction fatigue effects in line with existing models, but this effect was not evident for the driven cast-in-situ or screw injection piles. Finally, shaft and base resistances measured in the dense to very dense sand layers were greater than limiting resistances prescribed in several design standards. By taking this into consideration in design standards, the results would help reduce some of the overconservatism present in design and consequently reduce the financial and environmental cost of pile manufacturing and installation. **DOI: [10.1061/JGGEFK.GTENG-12026](https://doi.org/10.1061/JGGEFK.GTENG-12026).** *© 2024 American Society of Civil Engineers.*

Introduction

Dense to very dense sands are often considered as a competent load-bearing formation for piled foundations. Much of the industry focus has been brought to the design of piles of sand, for instance, because of growing wind energy development in the North Sea, an increased need to upgrade or renew port infrastructure (Roubos 2019), or intensifying urban development. However, there are several installation risks associated with dense sand. For instance, driven concrete and steel piles become prone to damage and risk not reaching their design depth (Randolph and Gouvernec 2011; de Gijt and Broeken 2013; Jardine 2020; Prendergast et al. 2020). For cast-in-situ piles, reusable steel casings can become stuck and irretrievable. Alternatively, the high radial stresses imposed by the soil can affect the pile shape and concrete quality, reducing the structural integrity of the piles (O'Neill 1991; Fleming et al. 2008). These risks create large financial and environmental costs and lead to severe project delays.

Different installation methods can help mitigate these risks. Water jetting during the installation of a driven precast (DP) pile can reduce the number of hammer blows needed and decrease the likelihood of pile damage. Screw injection (SI) piles inject grout from the pile tip during installation, reducing the shaft resistance on the casing as it screws into the ground. Driven cast-in-situ (DCIS) piles combine a reusable steel casing with an oversized base plate, reducing the shaft resistance on the pile during installation.

A reliable design method should account for these installation effects. Methods that link the pile base resistance q_b and pile shaft resistance q_s to the cone penetration test (CPT) tip resistance q_c have provided reliable estimates of the pile axial capacity (Jardine et al. 2005; Lehane et al. 2005; Lacasse et al. 2013). In the Netherlands, for example, the unit resistances are calculated using

$$q_b = \alpha_p q_{c,\text{avg}} \tag{1}$$

$$q_s = \alpha_s q_c \tag{2}$$

where α_p and α_s = correlation factors that depend on the pile type and installation method; and $q_{c,\text{avg}}$ = weighted average of cone resistances in a zone around the pile base, determined using algorithms such as the filter method (Boulanger and DeJong 2018) or the 4D/8D Dutch method (van Mierlo and Koppejan 1952; Reinders et al. 2016).

Adjustments to these two equations can account for different soil–structure interaction effects. For example, the new Unified design method for offshore driven piles (Lehane et al. 2020) includes a factor describing the cyclic degradation of shear stress during to pile driving, known as friction fatigue (Vesic 1970; Lehane et al. 1993; White and Bolton 2004; Gavin and O'Kelly 2007). This reduction is modeled as a function of the distance h from the pile base normalized by the pile (equivalent) diameter D_{eq}

$$\alpha_s \propto \left(\frac{h}{D_{\text{eq}}}\right)^{-c} \tag{3}$$

where c = constant that depends on the number of load cycles experienced during installation and the pile-end condition, to name but a few (Jardine et al. 2013; Anusic et al. 2019; Lehane et al. 2020). For cast-in-situ or bored piles, in contrast, this effect has been shown to be absent (Gavin et al. 2009). Yet for DCIS piles,

[1]Ph.D. Candidate, Dept. of Geoscience and Engineering, Delft Univ. of Technology, Stevinweg 1, 2628 CN Delft, Netherlands (corresponding author). ORCID: https://orcid.org/0000-0002-7918-2171. Email: k.duffy@tudelft.nl

[2]Professor of Subsurface Engineering, Dept. of Geoscience and Engineering, Delft Univ. of Technology, Stevinweg 1, 2628 CN Delft, Netherlands. ORCID: https://orcid.org/0000-0002-0741-1115

[3]Associate Professor in Geotechnical Practice, Dept. of Geoscience and Engineering, Delft Univ. of Technology, Stevinweg 1, 2628 CN Delft, Netherlands.

[4]Geotechnical Researcher, Deltares, Boussinesqweg 1, 2629 HV Delft, Netherlands. ORCID: https://orcid.org/0009-0008-7932-8733

[5]Senior Engineer, Port of Rotterdam Authority, Wilhelminakade 909, 3072 AP Rotterdam, Netherlands.

© ASCE 04024043-1 J. Geotech. Geoenviron. Eng.

J. Geotech. Geoenviron. Eng., 2024, 150(6): 04024043

the complex combination of load cycling during installation, concrete casting, and casing withdrawal means it is not clear if their ultimate capacity is affected by friction fatigue (Flynn and McCabe 2016, 2021).

Furthermore, some design methods limit the shaft or base capacity in high strength soils. These can be simple limiting thresholds, such as in the Netherlands (NEN 2017) and Belgium (NBN 2022), or they can also depend on the soil strength or relative density, such as in China [JGJ 94-2008 (MOHURD 2008)], France (AFNOR 2018), and the offshore design code (API 2011). Limitations are also introduced implicitly, for example, within the averaging methods used to determine $q_{c,avg}$ or through lower correlation factors. These limitations primarily came from the lack of reliable load tests performed in very dense sand (te Kamp 1977; Poulos et al. 2001), creating an uncertainty that also propagated toward coarser gravelly sand (Ganju et al. 2020). Although limiting resistances offer an apparent degree of safety, they can also lead to larger piles and create difficult and costly installation procedures.

In 2019, a test site was established in the port of Rotterdam, the Netherlands. The site is redolent of North Sea geological conditions, underlain by dense to very dense sands with q_c values of up to 80 MPa. Three different pile types were tested: driven precast, driven cast-in-situ, and screw injection piles. Each pile was instrumented along its full length with two types of fiber optic sensors and loaded in axial compression. As a result, the site gives a unique insight into the base and shaft response of full-scale piles in dense to very dense sand, allowing for a direct comparison of different pile types installed at the same test site. Using these test results, this paper aims to answer the following questions:

- How does the installation method affect the pile base and shaft response?
- Should limiting values be applied to pile base and shaft resistance?

By answering these questions, optimized pile design methods for dense to very dense sands can be developed, reducing the cost and installation risk associated with pile installation in very dense sand.

Experimental Program

Ground Conditions

The test site was located at the harbor of Amaliahaven in the port of Rotterdam, Netherlands (Fig. 1). The harbor was formed in 2013 from reclaimed land, created as part of an extension of the port into

the North Sea known as the Second Maasvlakte. The local geology has been well researched (Hijma et al. 2012; Vos et al. 2015), and a large amount of subsurface data from the site and the surrounding area are publicly available in electronic format (BRO 2023). The test piles were arranged in two rows, with at least 16 m between each pile (Fig. 1).

Prior to installation, one CPT was performed at the center of each location, and at least three more CPTs were made around 2 m away from each location. A selection of these CPT profiles is shown in Fig. 2.

For interpreting the pile tests, the soil profile has been divided into the Ground Units (GU) outlined in Table 1. The uppermost unit GU1 consists of around 10 m of fine to coarse reclaimed sand, followed by 8 m of very fine to fine sand from the marine-deposited Southern Bight Formation. Across GU1, the cone resistances vary from 5 to 20 MPa, with peaks of up to 50 MPa. Underlying this unit are marine and fluvially deposited soils, referred to as GU2. These are very closely spaced to closely spaced thin laminations of very fine sand and clay from the Holocene epoch Naaldwijk and Echteld Formations. A geological deposit known as the Wijchen Member defines the lower boundary of GU2: a 1-m bed of stiff clay with cone resistances between 1.5 and 2.0 MPa. This deposit has been incorporated into GU2.

The defining feature of the site is GU3, a dense to very dense sand present from around 27 m below the surface. This unit is a fluvial middle- to late-Pleistocene sand called the Kreftenheye Formation, a formation widespread across the Netherlands and the Dutch North Sea Sector (Rijsdijk et al. 2005; Hijma et al. 2012). At the test site, the formation is a poorly sorted slightly to moderately gravelly coarse silica sand. Its q_c values increase rapidly within the first 2 m of the unit to an average of 40 MPa. Peaks of up to 80 MPa are evident, although pockets of loose sand and clay also appear occasionally, for example at 34.5 m depth in Fig. 2.

Pile Descriptions

Three driven precast, four driven cast-in-situ, and four screw injection piles were installed and tested between October 2019 and January 2020. Each pile type has its own unique installation features that make installation easier in dense sand (Fig. 3). The piles were installed to a predefined depth at least $6.8D_{eq}$ into layer GU3 (Table 2).

Driven Precast Piles
The three 400-mm square prestressed DP piles (C90/105 concrete) were installed with a Junttan HHK12A hydraulic hammer (Kuopio,
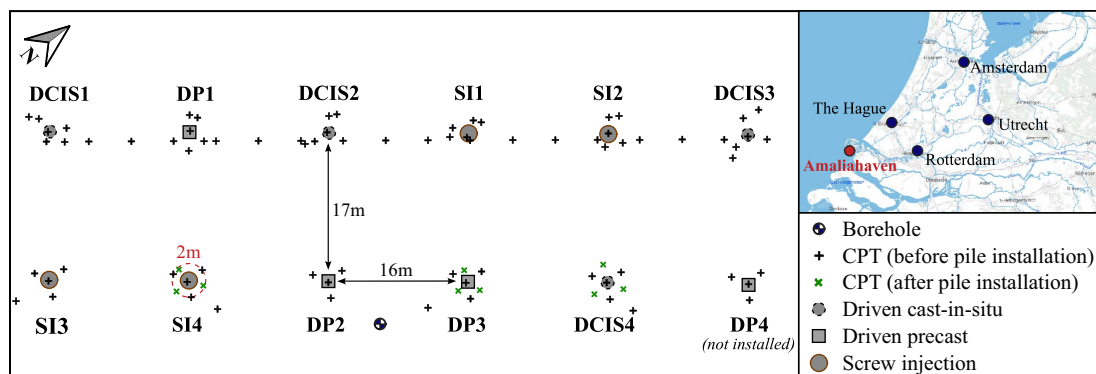
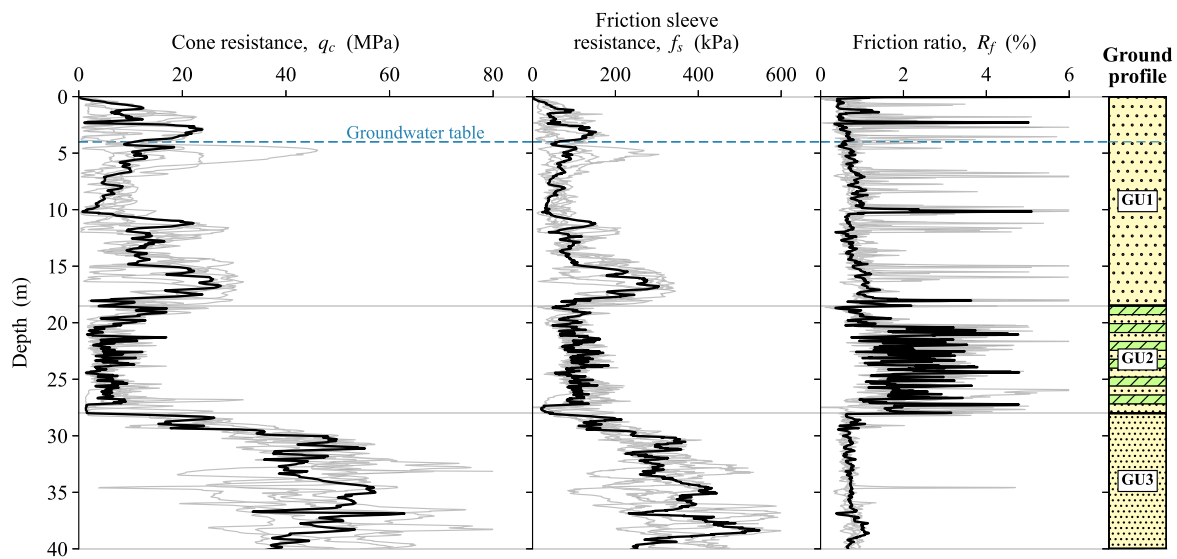**Fig. 1.** Layout and location of the Amaliahaven test site. [Map courtesy of PDOK, under Creative Commons-BY-4.0 license (https://creativecommons.org/licenses/by/4.0/).]

© ASCE 04024043-2 J. Geotech. Geoenviron. Eng.

J. Geotech. Geoenviron. Eng., 2024, 150(6): 04024043

Fig. 2. Selected CPT results across the test site and the interpreted ground units.

Table 1. Ground units used for the interpretation of the pile tests and results of in situ and laboratory tests

Unit	Soil type	Geological formation	Depth (m)	Mean q_c (MPa)	γ_t (kN/m³)	w_c (%)	w_L (%)	w_P (%)	s_u (kPa)	D_{50} (μm)	C_u	Gravel content (%)
GU1	Loose to dense very fine to coarse sand	Anthropogenic and Southern Bight Formation	0.0–18.5	14.5	19.9	21	—	—	—	159	2.6	0.0
GU2	Interlaminated clay and sand	Naaldwijk and Echteld Formations	18.5–27.0	6.4	18.7	32	40	24	228	65	23.9	0.0
GU2	Stiff clay	Wijchen Member	27.0–28.0	1.7	17.3	53	81	43	195	—	—	—
GU3	Coarse dense to very dense sand	Kreftenheye Formation	28.0–45.0	43.9	19	24	—	—	—	308	8.9	4.1

Note: γ_t = total unit weight; w_c = natural water content; w_L = liquid limit; w_P = plastic limit; s_u = undrained shear strength measured by consolidated undrained triaxial tests; D_{50} = mean particle size; C_u = coefficient of uniformity; and gravel content = percentage of particles retained on 2-mm sieve.
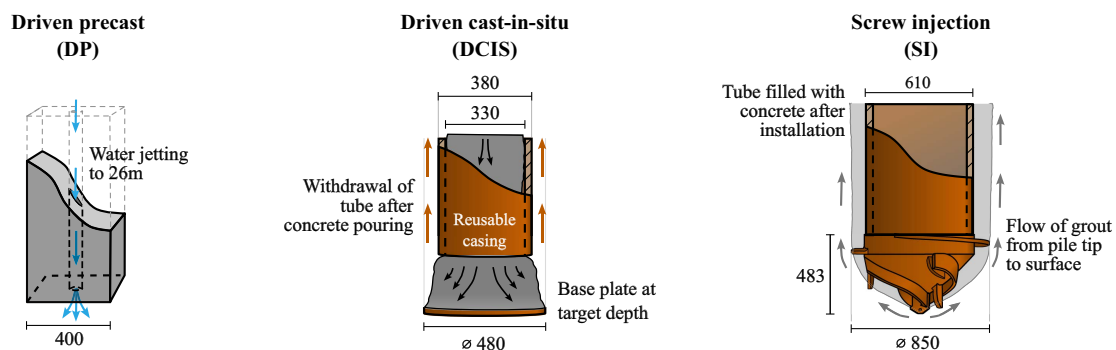

Fig. 3. Key installation features of the three pile types and their geometries. All dimensions are in millimeters unless otherwise stated.

Finland). During hammering, water jetting from the pile base was also performed until the piles reach 2 m above GU3. As a result, fewer than 50 blows per 25 cm were needed to penetrate GU1 and GU2 (Fig. 4), although the hammer energy (derived from the block weight and falling height) varied across the three piles in GU2. The blow count increased significantly as the pile penetrated through GU3 at 27 m depth, reaching up to 250 blows per 25 cm with comparable hammer energies across the three piles. In the end, each pile received around 2,300 blows in total.

Driven Cast-In-Situ Piles

The DCIS piles used a reusable steel casing with an outer diameter of 380 mm and a wall thickness of 25 mm. At the bottom of the casing, a sacrificial steel base plate was fitted to prevent soil from entering the casing. This base plate had an outer diameter of 480 mm, creating an offset of 50 mm with respect to the reusable steel casing. The casing and the base plate were then driven to the target depth using an IQIP S-120 hydraulic hammer (Sliedrecht, Netherlands). The piles experienced relatively easy driving in

© ASCE 04024043-3 J. Geotech. Geoenviron. Eng.

J. Geotech. Geoenviron. Eng., 2024, 150(6): 04024043

Table 2. Overview of the test piles

Pile	Equivalent diameter, D_{eq} (mm)[a]	Pile length, L (m)	$q_{c,avg}$ (MPa)[b]	Days between installation and testing
DP1	450	31.7	45.5	28
DP2	450	31.3	44.1	30
DP3	450	31.8	45.3	78
DCIS1	480	32.5	40.9	59
DCIS2	480	32.5	52.4	34
DCIS3	480	32.5	51.0	50
DCIS4	480	32.5	50.5	52
SI1	850	37.0	43.4	43
SI2	850	37.1	45.5	49 (retest: 95)
SI3	850	35.0	31.5	78
SI4	850	34.1	35.0	50

[a]Defined as the outermost diameter at the pile base for the DCIS and SI piles, equivalent diameter for the DP piles.
[b]Determined using an adjustment to the filter method of Boulanger and DeJong (2018), outlined by De Boorder et al. (2022).
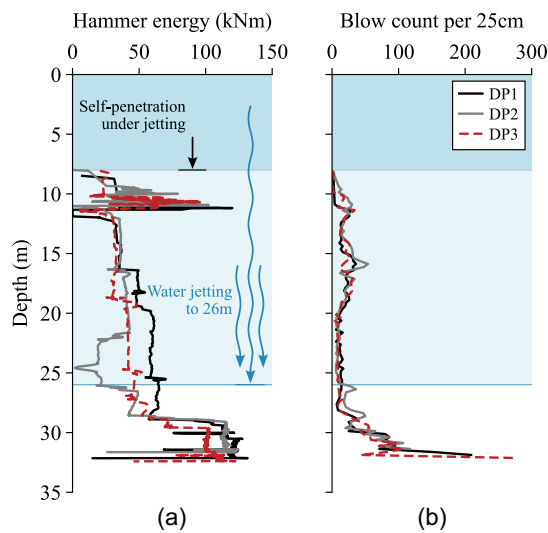
Fig. 4. Installation data from the driven precast piles.
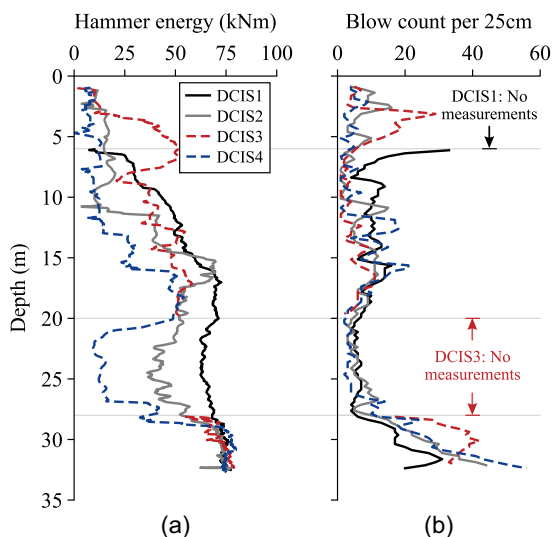
Fig. 5. Installation data from the driven cast-in-situ piles.

the upper layers, with blow counts of around 10 blows per 25 cm [Fig. 5(a)]. In GU3, the blow counts started to increase gradually with depth [Fig. 5(b)]. However over last few meters, the blow count began to reduce for piles DCIS1 and DCIS3, even though all DCIS piles were subjected to similar hammer energies.

Once the DCIS piles reached the target depth, it was checked that no water intruded between the casing and the base plate. The reinforcement cage (4×50-mm-diameter bars) was then placed inside the empty casing, followed by free-fall pouring of concrete (C35/45 XC2 S3, with maximum aggregate size of 8 mm) from the top of the casing. Finally, the casing was withdrawn using a reverse hammering action, leaving the base plate at the target depth.

Screw Injection Piles

The SI piles consisted of a steel tube (S355, 610-mm outer diameter, and wall thickness of 24 mm) welded to a larger 850-mm-diameter screw tip. The pile type is colloquially referred to as a Tubex pile and is part of a collection of pile types known as drilled displacement or screw displacement piles (Basu et al. 2010). SI piles are installed using a combination of a pulldown force and torque while grout is injected horizontally from the pile tip (Fig. 3). By injecting grout, soil around the pile tip is partly fluidized and can reduce the end-bearing resistance during installation. The mixture of grout and soil then flows up the annulus created by the enlarged screw tip, reducing the shaft resistance during installation. Upon hardening, the pile also benefits from an increased cross-sectional area.

To prevent fluidizing the soil underneath the pile base, the injection is then turned off across the final part of installation—in the case of the test site, several centimeters above the final pile tip depth. Unlike the more widely known Fundex pile, the steel tubes of the SI piles at the test site remained in situ after installation and were filled with concrete, essentially acting as a reinforced concrete pile.

Piles SI1 and SI2 were longer than SI3 and SI4 to investigate regions of higher and lower q_c around the pile base (Table 2). All piles used grout with a water-cement ratio of 2:1 and injected at a constant rate of 180 L/min across most of the installation depth, increasing to 215 and 200 L/min in the final 5 m of installation for piles SI3 and SI4, respectively. Pile SI2 penetrated at a higher rate through the first 20 m compared with the other three SI piles [Fig. 6(a)]. The penetration rate reduced in all piles to around 0.5 m/min through GU3, with SI2 penetrating slightly faster despite the higher grout injection rates of SI3 and SI4. Each pile required a total of 13 to 20 m³ of grout [Fig. 6(b)], although the grout flowing out at the ground surface could not be accurately quantified. All four SI piles were filled with C35/45 XC2 F4 concrete with maximum particle size of 16 mm.

Instrumentation

Test Frame

During testing, loads of up to 25 MN could be generated by a test frame tied-in by up to 12 self-boring anchors (Fig. 7). Each anchor was grouted in GU3 and inclined away from the pile to prevent any interaction between the pile and the anchors. The load tests then began at least 2 weeks after anchor installation to allow for grout curing. Six hydraulic jacks applied the load on the pile, distributed evenly across the pile head using a steel cap. A load cell on top of each jack measured the applied load Q_0, and four linear variable displacement transducers recorded the pile head displacement s_0. The displacement was measured relative to a reference frame
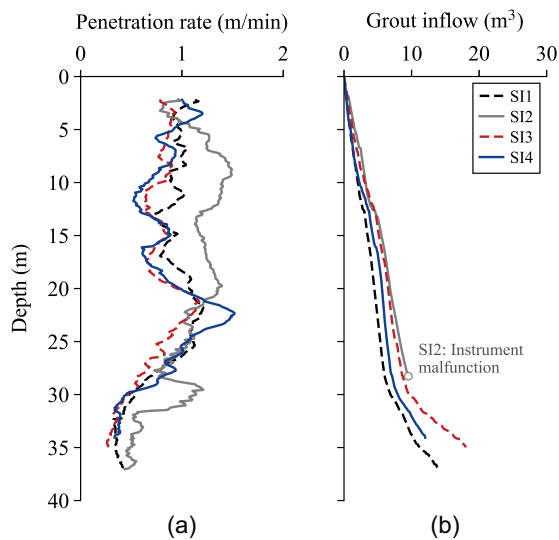
© ASCE 04024043-4 J. Geotech. Geoenviron. Eng.

J. Geotech. Geoenviron. Eng., 2024, 150(6): 04024043

Fig. 6. Installation data from the screw injection piles.

with supports 3.7 m away from the test pile. Inclination of the test frame was also monitored and controlled for during each test.

Strain Measurements

Two different types of fiber optic measurements recorded the change in strain along the pile: Fiber Bragg Grating (FBG) and Brillouin Optical Frequency Domain Analysis (BOFDA). At 19 different levels on each pile, a 1-cm-long FBG was etched onto a glass fiber–reinforced polymer fiber optic cable. At each FBG, a Luna Innovations sm125 interrogator (Roanoke, Virginia) provided a discrete strain measurement every 10 s. Conversely, the BOFDA system gave a continuous strain distribution along the full length of the pile with a spatial resolution of 20 cm. The BOFDA measurement was performed using the fibrisTerre fTB 2505 interrogator (Berlin) and the BRUsens V9 fiber optic cable (Solifos, Windisch, Switzerland). Compared with the FBG system, the BOFDA system measured at a slower frequency of every 4 min. To assess residual loads in the driven precast piles, temperature compensation was applied to the strain measurements using distributed fiber optic temperature sensing (Raman scattering). The temperature compensation process was outlined by Duffy et al. (2022).

The DP piles were the only piles to be instrumented prior to concrete casting in the manufacturing plant, with the fiber optic cables placed along the central axis of each DP pile. The DCIS

piles were instrumented onsite by attaching the fiber optic cables to opposite sides of the reinforcement cage. The instrumented cage was then placed in the empty reusable casing just before concrete pouring. The SI piles were instrumented after installation using two axially opposing reservation tubes on the inside of the primary steel tube. After placing the fiber optic cables in the reservation tubes, grout was then used to fix the cables in place.

Strain readings were converted to normal force using the tangent stiffness method by Fellenius (2001). For each pile, the derived stiffness agreed well with the theoretical stiffness, and the converted forces in the upper part of the piles were compatible with the forces measured by the load cells.

Pile Test Procedure

All piles were loaded in static compression, in general compliance with the Dutch guidance document for pile load tests (NEN 2020). Each pile was loaded in a minimum of eight steps, with each step being held for a minimum of 30 min and a maximum of 120 min. During each step, the creep rate at the pile head was assessed, and depending on this magnitude, the step was either prolonged or progressed to the next load step. The test ended when the pile base displaced by at least 10% of the pile's (equivalent) diameter, referred to as geotechnical failure. The first load test was performed on Pile DP1 and included an unload/reload cycle after each load step. Subsequent tests excluded load cycles unless they were required for operational reasons, for instance, if excessive inclination of the test frame created a safety risk.

Results

Load-Displacement Response

The following observations can be made from the load-displacement response of all piles (Fig. 8):

- The DP piles behaved very similarly and failed at loads between 8.0 and 8.6 MN [Fig. 8(a)]. The lowest capacity was reached by DP1, where load cycles were performed after each step. To investigate the effect of pile aging, Pile DP3 was tested 7 weeks after DP1 and DP2. However, Pile DP3 did not reach a higher failure load than the two other DP piles.
- The DCIS piles reached similar loads to the DP piles but showed more variability in the failure loads, ranging from 7.4 to 9.0 MN [Fig. 8(b) and Table 3]. Pile DCIS2 was the only DCIS pile not subjected to a load cycle and reached the highest capacity of
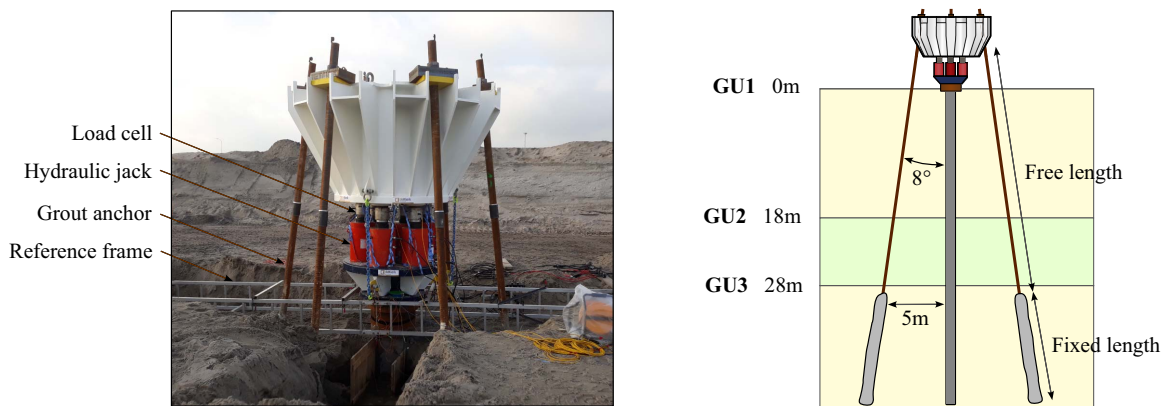

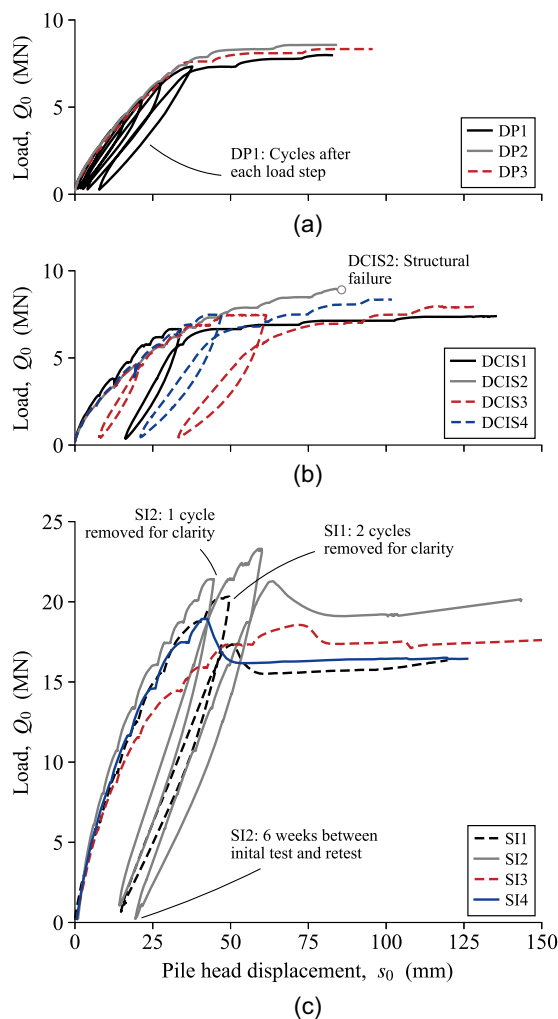**Fig. 7.** Test frame used to load the piles in axial compression.

© ASCE 04024043-5 J. Geotech. Geoenviron. Eng.

J. Geotech. Geoenviron. Eng., 2024, 150(6): 04024043

Fig. 8. Response of the pile head across each pile type.

Table 3. Peak resistances mobilized by each pile during testing

Pile	$Q_{0,max}$ (MN)	$q_{s,avg}$ (kPa)			q_b (MPa)
		GU1	GU2	GU3	
DP1	8.0	27	56	201	31
DP2	8.6	40	125	224	29
DP3	8.3	26	85	253	31
DCIS1	7.4	156	98	—	9
DCIS2	9.0	114	112	—	23
DCIS3	8.0	131	87	—	20
DCIS4	8.4	139	78	—	25
SI1	20.3	100	110	480	10
SI2	23.3	116	180	539	12
SI3	18.6	—	—	—	—
SI4	19.0	136	149	524	11

9 MN. However at this load, the concrete cracked just underneath the pile cap and so the pile could not be safely loaded to geotechnical failure.

- The SI piles mobilized the largest loads, reaching up to 24 MN. The longer piles, SI1 and SI2, reached higher capacities than the shorter piles, SI3 and SI4 [Fig. 8(c)]. When testing SI2, the reaction anchors began to deform as the load approached 24 MN, and the test had to stop before reaching geotechnical failure.

Before the retest 6 weeks later, fluidization of soil in GU1 and GU2 was attempted by flushing bentonite around the pile. This was done to reduce the shaft resistance in the two ground units so that the base and shaft resistance in GU3 could be fully mobilized within the capacity of the test frame. The retest reached a load of 21.5 MN, less than the maximum load in the initial test.

- At high test loads, each SI pile displaced very suddenly, and the previous peak load could not be reached again. The result is the softening response shown in the load-displacement curves, where the load reduced by up to 5 MN with increasing displacement. This response was also shown in the test on SI4 and the retest on SI2, both of which did not have any load cycles during the test. Under this reduced load, all piles reached the target base displacement.

Load Distribution

The BOFDA and FBG systems gave independent measurements of force with depth in the test piles (Fig. 9). These readings were collected for all piles except for Pile SI3 because of a breakage in the optical fibers. For the DCIS and SI piles, a zero-load condition was assumed at the start of testing because the curing grout or concrete could not lock in any of the residual stresses that may have developed during installation. In contrast, residual stresses were measured in the three DP piles at the start of each load test [Fig. 9(a)].

These residual stresses showed a similar trend with depth. At the surface, the load began with the weight of the test frame resting on the piles at the time of measuring. The load increased gradually with depth, most substantially in GU3, reaching a maximum load of 1.8 MN near the pile base. This base load corresponds to a stress of approximately 10 MPa, or 20% of $q_{c,avg}$ (Table 2). To balance this residual base stress, Fig. 9(a) suggests that each pile mobilized negative shear stresses along the entire pile length, acting in equilibrium with the load underneath the pile base. No time-dependent effects were evident in the residual stress measurements, and Pile DP3 exhibited a similar trend to DP1 and DP2 even though the residual stress measurement were performed 7 weeks later.

Fig. 9 also presents the load distributions at the highest applied load on the pile, with residual loads included in the distributions of the DP piles. For all three pile types, the reduction of force with depth was relatively constant in GU1 and GU2. In GU3, the slope of the distribution changed suddenly. For the DP and SI piles, the sharp reduction in force shows that the two pile types mobilized much more shaft resistance in GU3 than in GU1 or GU2. Surprisingly, the DCIS piles showed a very different pattern in GU3, with both the BOFDA and FBG readings showing a lot of noise and an apparent increase in force with depth.

It is not certain what was the true response of the DCIS piles in GU3 because the piles were not extracted after testing. The magnitude and scatter of the measured forces suggests that there was little to no concrete present in the piles across GU3. This problem has been observed before with driven cast-in-situ piles embedded in dense to very dense sand (van Weele and Lencioni 1999). Those authors provided several possible explanations for this, for example, low workability of the concrete mix, congestion created by the reinforcement cage, or the influence of surrounding soil and groundwater on the curing concrete.

In the case of the test piles presented in this paper, the DCIS piles used a larger-than-normal reinforcing cage to reduce the likelihood of structural failure during load testing. The size of the cage left little room for concrete pouring, and both the cage and the casing may have trapped coarse aggregates or cement particles during pouring, abetted by the large falling height of the concrete mix.

© ASCE 04024043-6 J. Geotech. Geoenviron. Eng.

J. Geotech. Geoenviron. Eng., 2024, 150(6): 04024043
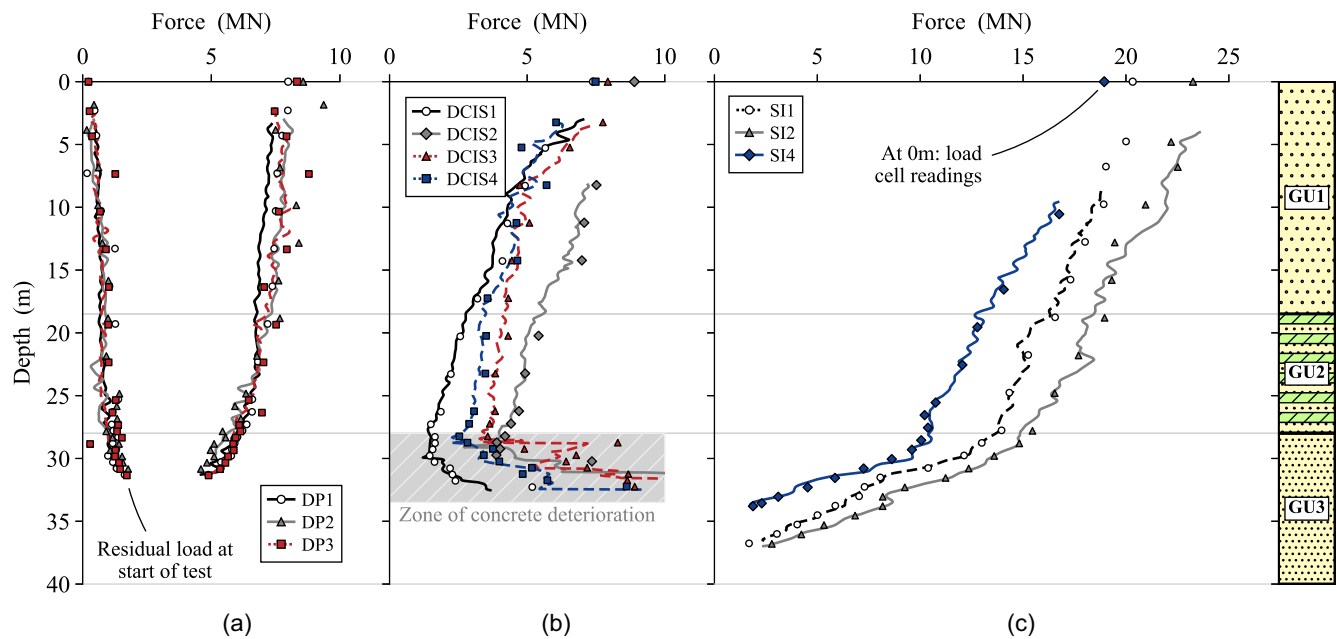
Fig. 9. Load distribution at peak load $Q_{0,\max}$ of all piles as well as the residual load in the DP piles at the start of testing. BOFDA readings are represented by continuous lines, and FBG readings by discrete points.

The fact that scattering in the strain readings was coincident with the layer boundary between GU2 and GU3 may also suggest an influence of the local ground conditions. For instance, the hydrostatic pressure created by the wet concrete column may not have been enough to resist the high radial stresses imposed by GU3 after casing removal. Both scenarios would have led to poor concrete quality at the bottom of the pile, and it is expected that little to no concrete was present across GU3, causing much higher and more variable strain measurements in this ground unit. Consequently, in this analysis, it has been assumed that no shaft friction could develop over GU3 and instead, the load at the GU2–GU3 interface was transferred directly through the reinforcement and onto the base plate.

Because good agreement was shown in all piles between the BOFDA and FBG readings, only the FBG readings are considered herein due to their higher measurement frequency and accuracy.

Shaft Resistance

To calculate the average shaft resistance $q_{s,\mathrm{avg}}$, the change in normal force across a ground unit was taken. To convert this force to shaft resistance, the outermost diameter of the DCIS (= 480 mm) and SI piles (= 850 mm) was used. Table 3 summarizes the results for all test piles and a selection of mobilization curves are presented in Fig. 10.
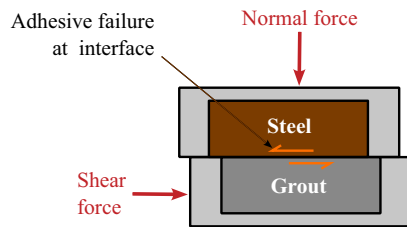
Installation-induced negative shear stresses were measured in all three ground units at the beginning of the driven precast pile tests. These stresses were greatest in GU3, where around −80 kPa of shear stress was acting on the piles at the start of testing compared with only −20 kPa of shear stress in GU1. During the load tests, the DP piles mobilized low shaft resistances in GU1, with peak resistances of around 30 kPa [Fig. 10(a)]. On the other hand, the DCIS and SI piles reached much higher shaft resistances in GU1, ranging from 100 to 156 kPa. The two pile types mobilized this peak resistance at a slower rate than the DP piles, at displacements of around 4% (DCIS piles: 19 mm; SI piles: 34 mm) of the pile diameter, compared with 1.5% (7 mm) for the DP piles, where the
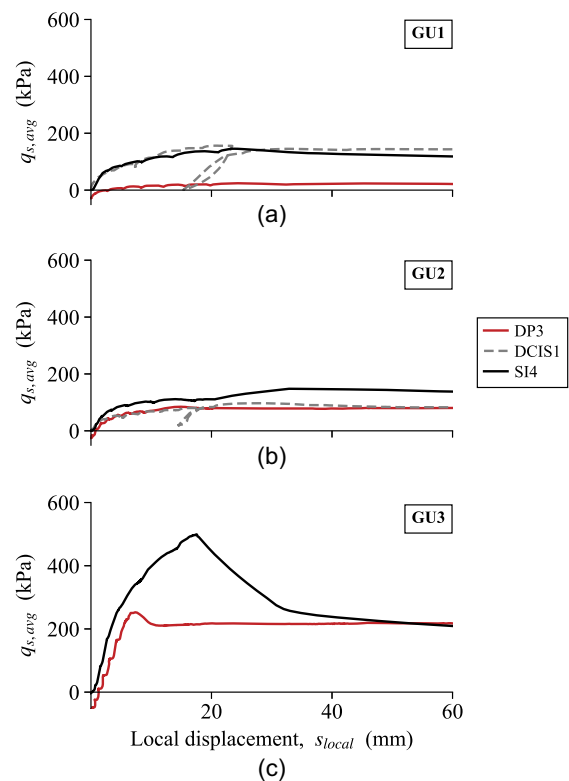
Fig. 10. Mobilized shaft resistances of selected piles in (a) GU1; (b) GU2; and (c) GU3.

stresses reversed from being in tension at the start of testing to under compression at the maximum applied test load.

A similar response was shown by all three pile types in the mixed soil unit GU2 [Fig. 10(b)]. The highest peak resistances were recorded by the SI piles with an average of around 145 kPa, whereas the DP piles recorded the lowest of around 90 kPa.

© ASCE 04024043-7 J. Geotech. Geoenviron. Eng.

J. Geotech. Geoenviron. Eng., 2024, 150(6): 04024043

Fig. 11. Schematic of the direct simple shear test to test bond strength.

Fig. 12. Mobilized base resistance across all piles, including the residual stress contribution of the DP piles. For clarity, loading cycles have been removed.

However, the rate at which these peak resistances were mobilized was similar across the three pile types.

Very high shaft resistances were measured in the dense to very dense sand layer, GU3. The DP piles recorded peak resistances of 201 to 253 kPa, occurring within a displacement of 7 mm or 1.5% of the equivalent diameter [Fig. 10(c)]. Interestingly, Pile DP3 showed softening behavior in its response, with the shaft resistance reducing from a peak of 253 to 215 kPa. This softening response was not exhibited by the two other DP piles, tested 7 weeks earlier.

The SI piles mobilized high shaft resistances in GU3, ranging from 480 to 539 kPa and mobilizing at displacements of 15–20 mm, 2% of the pile diameter. Notably, a sharp reduction in shaft resistance occurred with increasing displacement, corresponding with the postpeak reduction observed in the total load-displacement curves [Fig. 8(c)].

To investigate the cause of this sharp reduction, direct simple shear tests were performed to investigate the adhesive strength of the steel-grout interface and to see if debonding could have occurred between to the two materials (Fig. 11). Seven samples were prepared to capture potential changes in steel roughness and grout water-cement ratio due to installation. Three samples were tested on smooth steel (roughness $\approx 4~\mu$m) and four samples on rough steel (roughness $\approx 32~\mu$m), with the water-cement ratio ranging from 1:1 to 2:1 within both groupings. Each sample was first sheared at a low normal stress, and if adhesive failure did not occur at the interface, the normal stress was then increased incrementally toward magnitudes expected for the test site. Six of the seven samples failed at a normal stress of 1,459 kPa. At this normal stress, the four rough steel samples failed at shear stresses ranging from 927 to 1,222 kPa and two smooth samples failed at shear stresses of 379 and 500 kPa. The last remaining smooth sample failed at a normal stress of 912 kPa and a shear stress of 312 kPa.

The laboratory results indicate that the shear stresses reached in GU3 during pile testing were close to the ultimate bond strength of the steel–grout interface. As a result, it is likely that adhesive failure occurred in GU3 at the steel–grout interface, causing a sharp reduction in the shaft resistance in the soil unit. No adhesive failure occurred in GU1 and GU2 due to the low shear stresses mobilized in the two soil units (<160 kPa), less than the lowest shear stress at failure during the laboratory tests.

Base Resistance

The base resistance of the piles was extrapolated from the lowest FBG measurement, generally within one pile diameter from the pile base. This resistance was then converted to a stress using the outermost diameter of the DCIS (= 480 mm) and SI piles (= 850 mm). A wide spectrum of responses was recorded across the three pile types (Fig. 12 and Table 3). The DP piles mobilized the highest base resistances, building up from a residual stress of 10 MPa at the start of testing, to peak capacities of around 30 MPa. This peak resistance developed quickly, within a base displacement of 30 mm.
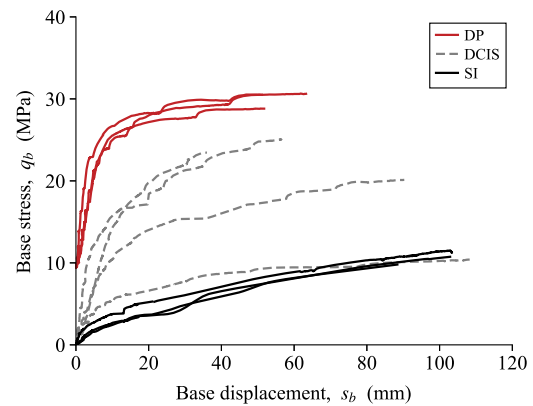
Some variability in the assumed base resistances of the DCIS piles was exhibited, ranging from 10 to 25 MPa. Two DCIS piles behaved very similarly upon loading, reaching peak capacities of up to 25 MPa. In contrast, DCIS1 only mobilized a base stress of 10 MPa, and the other pile, DCIS3, exhibited a response in between the two extremes. Given the likely absence of concrete in the lower section of the pile and the resulting transfer of load through the reinforcing cage, such variability is likely due to installation problems rather than a real pile response.

The SI piles mobilized the lowest base resistances of the three pile types, reaching peak resistances of 10 to 12 MPa—just one-third of the base resistance recorded by the DP piles. All three of the SI piles mobilized their resistance at a very similar rate, a rate much slower than the DP and DCIS piles. Fig. 12 also suggests that some additional capacity could have been mobilized if the SI piles were displaced further.

Discussion

Limiting Resistances

By instrumenting and load testing piles in the dense to very dense sands of the test site, some unique data points have been collected to understand pile behavior at high cone resistances. Of the three pile types tested, the DP piles recorded the largest base resistances of around 30 MPa (Fig. 12). For example, this is twice as much as the 15 MPa limitation in the Dutch design standard (NEN 2017) and the 12 MPa limitation in the offshore design code (API 2011). The residual base stresses (= 10 MPa) were a substantial component of the base response of each DP pile, measuring one-third of their peak base capacity. These residual stresses alone bring the base resistance close to existing limitations and if neglected, would cause significant misinterpretation of the ultimate pile base capacity. Three of the four DCIS piles also reached base resistances greater than 15 MPa.
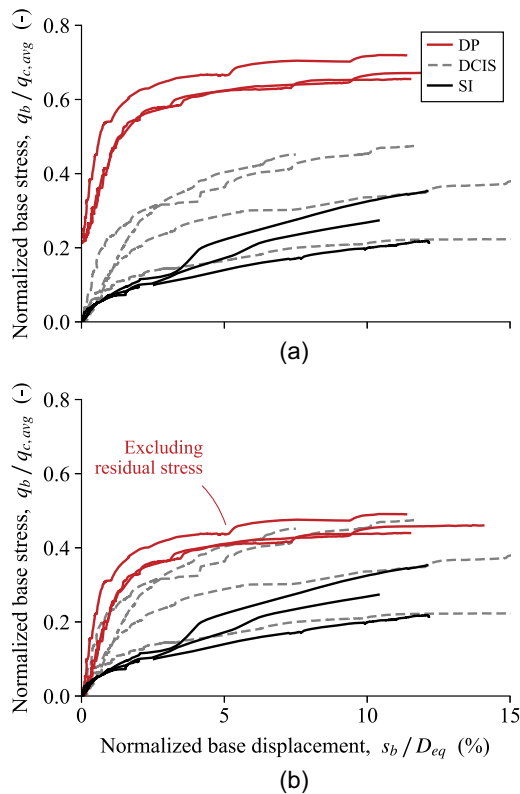
Similar inferences can be made in terms of limiting shaft resistances. The DP piles mobilized resistances of around 200 kPa in GU3, greater than the 150 kPa limitation in the Dutch design standard or the 115 kPa limitation in the offshore design code. The DCIS piles also mobilized resistances just under their prescribed limiting resistances (= 210 kPa in the Dutch design code), even though the shaft resistance of the DCIS piles was only assessed in the looser GU1 and GU2 ground units.

© ASCE   04024043-8   J. Geotech. Geoenviron. Eng.

J. Geotech. Geoenviron. Eng., 2024, 150(6): 04024043

The largest and longest piles tested, the SI piles, reached shaft resistances of more than 500 kPa across GU3 and greatly exceeded prescribed limiting resistances. However at these stresses, structural failure occurred at the grout–steel interface and greatly reduced the available shaft resistance. This suggests that the geotechnical capacity is not limited within the range of shear stresses measured in the presented pile tests, although allowances for the structural capacity of the pile should still be made, particularly for piles with complex structural interfaces.

Normalized Base Resistance

Fig. 13 compares the base response of the three pile types by normalizing with D_{eq} and $q_{c,avg}$ (Table 2). The DP piles developed the highest normalized base resistance α_p of between 0.65 and 0.75, with residual stresses included. In comparison, the DCIS piles showed a much more diverging behavior, with α_p ranging from 0.20 to 0.45. Part of this diverging behavior may reflect a variation in soil conditions around the pile base. It could also suggest some sensitivity of the DCIS base response to the surrounding soil and installation conditions. For instance, the pile base of DCIS2 and DCIS4 responded quite similarly during testing, and both piles also experienced a high number of hammer blows toward the end of installation (Fig. 5).

On the contrary, the blow count reduced over the final couple of meters for DCIS1 and DCIS3, with both piles also recording much lower α_p values. Just like the DP piles, it would be expected that the DCIS piles would also develop some residual base stress after installation given the similarity in installation processes. However, the removal of the reusable casing and placement of wet concrete would resul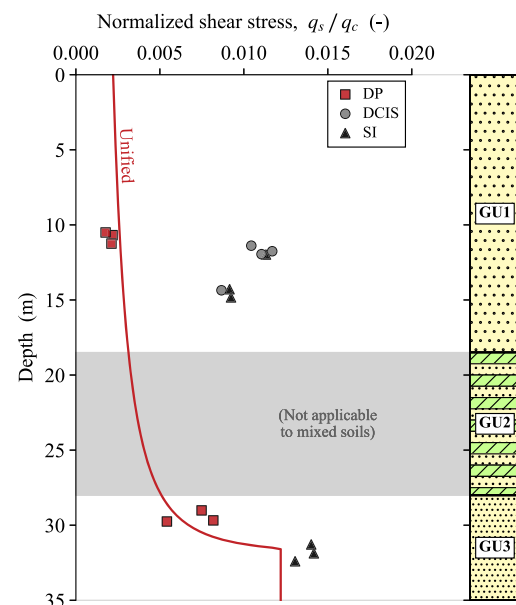t in the upward movement of the base plate until the residual base stress and the self-weight of the concrete column reached an equilibrium. Consequently, Piles DCIS2 and DCIS4 responded quite similarly to the DP piles with residual loads excluded [Fig. 13(b)], with very similar α_p values at a normalized displacement of 10%.

The SI piles mobilized the lowest α_p values of between 0.20 and 0.35. The rate at which the SI piles reached these peak values was also much slower than the DCIS and DP piles. For instance, the DP piles mobilized almost all their base capacity within 3% D_{eq} but at the same displacement, the SI piles mobilized only 30% of their base capacity. This slow response of the SI piles resembled more a bored pile than a displacement pile. The α_p values reached were also lower than the typical range of 0.63–0.70 listed in design standards (NEN 2017; NBN 2022).
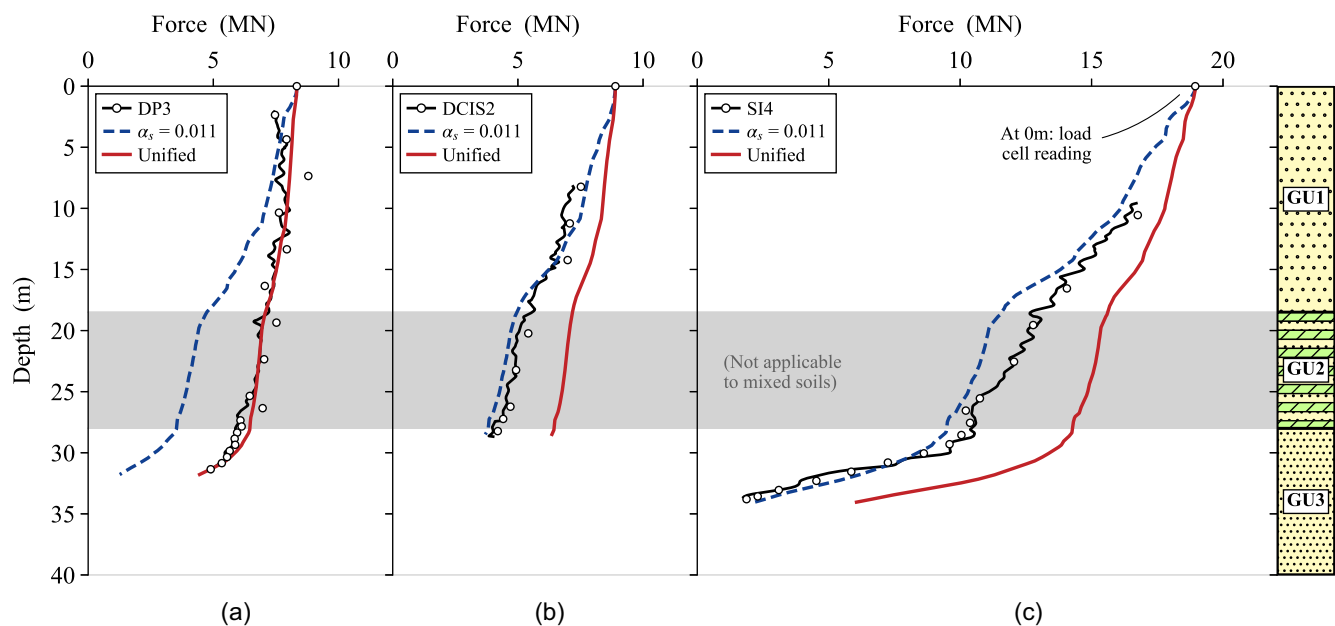
Normalized Shaft Resistance

Fig. 14 compares the normalized peak shear stresses α_s of the three pile types in the two clean sand layers, GU1 and GU3. Toward the bottom of the pile, the DP piles recorded α_s values 50% lower than those mobilized by the SI piles. This difference was even more substantial toward the top of the pile, with the same DP piles mobilizing resistances three to four times lower than the SI and DCIS piles. This variation with depth in normalized shaft resistance is modeled well by the Unified design method (Lehane et al. 2020), which includes a friction fatigue term [Eq. (3)] to describe the cyclical degradation of shaft friction caused by pile installation. In contrast, less variation in the SI piles was exhibited across their length, with slightly higher α_s mobilized in GU3 compared with GU1 at h/D_{eq} of 20 to 30. In GU1, the DCIS piles mobilized significantly greater α_s values than the DP piles, reaching values similar to the SI piles.

Further insight into the distribution of shaft resistance with depth for all piles is given in Fig. 15. This figure compares the measured load-depth profile at the peak mobilized pile capacity $Q_{0,max}$. The actual distribution is compared with that predicted using either a constant α_s [Eq. (2)] or an α_s value that varies with h/D as per the Unified design method. The predicted load at a given depth is

Fig. 13. Comparison of the normalized base resistance across all piles: (a) with residual loads included in the DP piles; and (b) with residual loads excluded in the DP piles.

Fig. 14. Normalized peak shear stress of all piles in GU1 and GU3, including residual load in the DP piles.

© ASCE

04024043-9

J. Geotech. Geoenviron. Eng.

J. Geotech. Geoenviron. Eng., 2024, 150(6): 04024043

Fig. 15. Measured load distribution compared with different design methods. The load cell reading is taken as a fixed point from which the design shaft resistance is subtracted.

calculated by subtracting the cumulative predicted shaft resistance to that depth from the maximum measured load resistance at the pile head. The conclusions for each pile type are as follows:

- For the DP piles, the Unified method predicted the shaft resistance very accurately over the entire pile length, including in GU1 and GU2, where water jetting was performed. In contrast, adoption of a constant α_s resulted in an overestimation of shaft resistance.
- For the DCIS piles, the Unified method underestimated the shaft resistance with depth. In contrast, adoption of a constant α_s agreed well with the measured data. Even though the DCIS piles were also installed by driving, the results suggest that the shaft resistance measured during static loading was not affected by friction fatigue in spite of the high slenderness of the piles. The likely reason for this is because the geometry of the DCIS piles creates an offset between the base plate and the reusable casing (Fig. 3). This means that any friction fatigue effects created from pile driving will occur at the interface between the reusable casing and the soil. Following installation, this casing is withdrawn and the remaining void is filled with concrete, meaning that the shear interface during pile load testing is not the same as the interface that may have been affected by friction fatigue during installation.
- For the SI piles, a constant α_s provided a good prediction of the load distribution shown in Fig. 15. However the Unified method underestimated the shaft resistance, most significantly as the distance from the pile tip increased. This is unsurprising, given the significantly different mechanisms occurring during the installation of a SI pile compared with a driven pile.

Conclusion

Driven precast, driven cast-in-situ, and screw injection piles were installed at a test site in the Netherlands. The site was underlain by dense to very dense sands with CPT cone resistances of up to 80 MPa, similar to soil conditions across the Dutch North Sea sector. Each pile was instrumented with two types of fiber optic systems and loaded under axial compression to failure, meaning

that the base and shaft response of each pile could be clearly distinguished. As a result, the tests provide a unique data set where the influence of different installation methods on pile response can be compared when the piles are installed in very similar ground conditions. The main findings from the tests are as follows:

- The installation of the driven precast piles created large residual base stresses, mobilizing all the upper soil layers in negative shaft friction. Upon loading, the driven precast piles mobilized their maximum base resistance at relatively low displacements. On the contrary, the screw injection piles exhibited a much softer response, with much higher displacements needed to mobilize the maximum base resistance.
- The normalized shaft resistance of the driven precast piles showed variation with depth. This was in line with design methods describing friction fatigue, even though water jetting was performed in the upper soil layers. Conversely, no friction fatigue effect was shown by the shaft response of the driven cast-in-situ and screw injection piles.
- Very high base and shaft capacities were recorded during testing, greater than limiting resistances prescribed in some design standards. This suggests that these limitations introduce excessive conservatism into pile design when applied in dense to very dense silica sands. Nevertheless, the structural performance of the pile under high loads should be carefully considered.

Based on these findings, pile design could be optimized for quay wall development across the port of Rotterdam, leading to both environmental and financial savings while minimizing installation risks. Furthermore, by combining the test results with existing load test databases, a comprehensive overview can be made of the axial response of each pile type in sand along with investigating the appropriate design methods.

Data Availability Statement

Some or all data, models, or code that support the findings of this study are available from the corresponding author upon reasonable request.

Acknowledgments

Notation

The following symbols are used in this paper:

C_u = coefficient of uniformity;

c = calibration constant used in determining q_s;

D_{eq} = (equivalent) pile diameter;

D_{50} = mean particle size;

f_s = cone penetration test friction sleeve resistance;

h = distance from the pile base;

L = pile length;

Q_0 = load applied on the pile head;

$Q_{0,max}$ = highest load applied on the pile head;

q_b = pile base resistance;

q_c = cone penetration test tip resistance;

$q_{c,avg}$ = weighted average of cone tip resistances for determining the pile base resistance;

q_s = pile shaft resistance;

$q_{s,avg}$ = average pile shaft resistance across a ground unit;

R_f = cone penetration test friction ratio;

s_b = pile base displacement;

s_{local} = local shaft displacement;

s_u = undrained shear strength;

s_0 = pile head displacement;

w_c = natural water content;

w_L = liquid limit;

w_P = plastic limit;

α_p = correlation factor for determining the pile base resistance ($= q_{c,avg}/q_b$);

α_s = correlation factor for determining the pile shaft resistance ($= q_c/q_s$); and

γ_t = total unit weight.

Supplemental Materials

Table S1, Figs. S1–S5, and additional cone penetration tests and laboratory test data are available online in the ASCE library (www.ascelibrary.org).

References

AFNOR (French Standardisation Association). 2018. *Justification des ouvrages géotechniques-Normes d'application nationale de l'Eurocode 7-Fondations profondes [Justification of geotechnical work–National application standards for the implementation of Eurocode 7–Deep foundations].* [In French.] NF P94-262/A1. Paris: AFNOR.

Anusic, I., B. M. Lehane, G. R. Eiksund, and M. A. Lingaard. 2019. "Evaluation of installation effects on set-up of field displacement piles in sand." *Can. Geotech. J.* 56 (4): 461–472. https://doi.org/10.1139/cgj-2017-0730.

API (American Petroleum Institute) 2011. *Recommended practice for planning, designing, and constructing fixed offshore platforms–Working stress design.* API RP 2GEO. Washington, DC: API.

Basu, P., M. Prezzi, and D. Basu. 2010. "Drilled displacement piles–Current practice and design." *J. Deep Found. Inst.* 4 (1): 3–20. https://doi.org/10.1179/dfi.2010.001.

Boulanger, R. W., and J. T. DeJong. 2018. "Inverse filtering procedure to correct cone penetration data for thin-layer and transition effects." In *Proc., 4th Int. Symp. Cone Penetration Testing (CPT18)*, 24–44. Boca Raton, FL: CRC Press.

BRO (National Key Registry for the Subsurface). 2023. "BRO: Transparent, clear, accessible." Accessed November 23, 2023. https://basisregistratieondergrond.nl.

de Boorder, M., D. A. de Lange, and K. G. Gavin. 2022. "An alternative CPT averaging procedure to estimate pile base capacity." In *Proc., 11th Int. Conf. Stress Wave Theory and Design and Testing Methods for Deep Foundations*. Rotterdam, Netherlands: Zenodo. https://doi.org/10.5281/zenodo.7142197.

de Gijt, J., and M. L. Broeken. 2013. *Quay walls.* Leiden, Netherlands: CRC Press.

Duffy, K. J., K. G. Gavin, D. A. de Lange, and M. Korff. 2022. "Residual stress measurement of driven precast piles using distributed fibre optic sensors." In *Proc., 11th Int. Conf. Stress Wave Theory and Design and Testing Methods for Deep Foundations*. Rotterdam, Netherlands: Zenodo. https://doi.org/10.5281/zenodo.7146663.

Fellenius, B. 2001. "From strain measurements to load in an instrumented pile." *Geotech. News Mag.* 19 (1): 35–38.

Fleming, W. G. K., A. Weltman, K. Elson, and M. F. Randolph. 2008. *Piling engineering.* London: Taylor & Francis.

Flynn, K. N., and B. A. McCabe. 2016. "Shaft resistance of driven cast-in-situ piles in sand." *Can. Geotech. J.* 53 (1): 49–59. https://doi.org/10.1139/cgj-2015-0032.

Flynn, K. N., and B. A. McCabe. 2021. "Applicability of CPT capacity prediction methods to driven cast-in-situ piles in granular soil." *J. Geotech. Geoenviron. Eng.* 147 (2): 04020170. https://doi.org/10.1061/(ASCE)GT.1943-5606.0002445.

Ganju, E., F. Han, M. Prezzi, and R. Salgado. 2020. "Static capacity of closed-ended pipe pile driven in gravelly sand." *J. Geotech. Geoenviron. Eng.* 146 (4): 04020008. https://doi.org/10.1061/(ASCE)GT.1943-5606.0002215.

Gavin, K. G., D. Cadogan, and P. Casey. 2009. "Shaft capacity of continuous flight auger piles in sand." *J. Geotech. Geoenviron. Eng.* 135 (6): 790–798. https://doi.org/10.1061/(ASCE)GT.1943-5606.0000073.

Gavin, K. G., and B. C. O'Kelly. 2007. "Effect of friction fatigue on pile capacity in dense sand." *J. Geotech. Geoenviron. Eng.* 133 (1): 63–71. https://doi.org/10.1061/(ASCE)1090-0241(2007)133:1(63).

Hijma, M. P., K. M. Cohen, W. Roebroeks, W. E. Westerhoff, and F. S. Busschers. 2012. "Pleistocene Rhine–Thames landscapes: Geological background for hominin occupation of the southern North Sea region." *J. Quat. Sci.* 27 (1): 17–39. https://doi.org/10.1002/jqs.1549.

Jardine, R. J. 2020. "Geotechnics, energy and climate change: The 56th Rankine Lecture." *Géotechnique* 70 (1): 3–59. https://doi.org/10.1680/jgeot.18.RL.001.

Jardine, R. J., F. Chow, R. Overy, and J. Standing. 2005. *ICP design methods for driven piles in sands and clays.* London: Thomas Telford.

Jardine, R. J., B. T. Zhu, P. Foray, and Z. X. Yang. 2013. "Interpretation of stress measurements made around closed-ended displacement piles in sand." *Géotechnique* 63 (8): 613–627. https://doi.org/10.1680/geot.9.P.138.

Lacasse, S., F. Nadim, K. H. Andersen, S. Knudsen, U. K. Eidsvig, G. L. Yetginer, T. Guttormsen, and A. Eide. 2013. "Reliability of API, NGI, ICP and Fugro axial pile capacity calculation methods." In *Proc., Offshore Technology Conf.* New York: Curran Associates.

Lehane, B. M., et al. 2020. "A new 'unified' CPT-based axial pile capacity design method for driven piles in sand." In *Proc., 4th Int. Symp. on*

© ASCE   04024043-11   J. Geotech. Geoenviron. Eng.

J. Geotech. Geoenviron. Eng., 2024, 150(6): 04024043

Frontiers in Offshore Geotechnics, 462–477. Austin, TX: Deep Foundations Institute.

Lehane, B. M., R. J. Jardine, A. J. Bond, and R. Frank. 1993. "Mechanisms of shaft friction in sand from instrumented pile tests." *J. Geotech. Eng.* 119 (1): 19–35. https://doi.org/10.1061/(ASCE)0733-9410(1993)119:1(19).

Lehane, B. M., J. A. Schneider, and X. Xu. 2005. *A review of design methods for offshore driven piles in siliceous sand*. Perth, Australia: Univ. of Western Australia.

MOHURD (Ministry of Housing and Urban and Rural Development of the People's Republic of China). 2008. *Technical code for building pile foundations*. [In Chinese.] JGJ 94-2008. Beijing: MOHURD.

NBN (Belgian Bureau of Normalisation). 2022. *Eurocode 7: Geotechnisch ontwerp–Deel 1: Algemene regels [Eurocode 7: Geotechnical design–Part 1: General rules]*. [In Dutch.] NBN EN 1997-1 ANB:2022. Brussels, Belgium: NBN.

NEN (Dutch Standardisation Insitutue). 2020. *Geotechniek-Bepaling van het axiaal draagvermogen van funderingspalen door middel van proefbelastingen [Geotechnics–Determination of the axial capacity of foundations pile through load tests]*. [In Dutch.] NPR 7201:2017 +A1. Delft, Netherlands: NEN.

NEN (Dutch Standardisation Institute). 2017. *Geotechnisch ontwerp van constructies–Deel 1: Algemene regels [Geotechnical design of structures–Part 1: General rules]*. [In Dutch.] NEN 9997-1+C2. Delft, Netherlands: NEN.

O'Neill, M. W. 1991. "Construction practices and defects in drilled shafts." In *Integrity testing of foundations*, 6–14. Washington, DC: National Research Council.

Poulos, H. G., J. P. Carter, and J. C. Small. 2001. "Foundations and retaining structures–Research and practice." In *Proc., 15th Int. Conf. on Soil Mechanics and Foundation Engineering*, 2527–2606. Istanbul, Turkey: Balkema.

Prendergast, L. J., P. Gandina, and K. G. Gavin. 2020. "Factors influencing the prediction of pile driveability using CPT-based approaches." *Energies* 13 (12): 3128–3147. https://doi.org/10.3390/en13123128.

Randolph, M. F., and S. Gouvernec. 2011. *Offshore geotechnical engineering*. Oxford, UK: Spon Press.

Reinders, K., A. van Seters, and M. Korff. 2016. "Design of piles according to Eurocode 7–Dutch practice." In *Proc., ISSMGE-ETC 3 Int. Symp. Design Piles Europe*. London: International Society for Soil Mechanics and Geotechnical Engineering.

Rijsdijk, K. F., S. Passchier, H. J. T. Weerts, C. Laban, R. J. W. van Leeuwen, and J. H. J. Ebbing. 2005. "Revised upper cenozoic stratigraphy of the Dutch sector of the North Sea Basin: Towards an integrated lithostratigraphic, seismostratigraphic and allostratigraphic approach." *Neth. J. Geosci.* 84 (2): 129–146. https://doi.org/10.1017/S0016774600023015.

Roubos, A. 2019. "Enhancing reliability-based assessments of quay walls." Ph.D. thesis, Dept. of Hydraulic Engineering, Delft Univ. of Technology.

te Kamp, W. G. B. 1977. "Sonderen en funderingen op palen in zand" [CPTs and piled foundations in sand]. [In Dutch.] In *Proc., Sondeer Symp, 1977*, 119–133. Utrecht, Netherlands: Fugro.

van Mierlo, W., and A. Koppejan. 1952. *Lengte en draagvermogen van heipalen.* [*Length and bearing capacity of driven piles*]. [In Dutch.] Rotterdam, Netherlands: Stichting Bouw.

van Weele, A. F., and B. M. L. G. Lencioni. 1999. "Het mislukken van een paalfundering is duur, maar leerzaam." [In Dutch.] In *Geotechniek*. Rotterdam, Netherlands: Uitgeverij Educom.

Vesic, A. S. 1970. "Tests on instrumented piles, Ogeechee River site." *J. Soil Mech. Found. Div.* 96 (2): 561–584. https://doi.org/10.1061/JSFEAQ.0001404.

Vos, P. C., F. P. M. Bunnik, K. M. Cohen, and H. Cremer. 2015. "A staged geogenetic approach to underwater archaeological prospection in the Port of Rotterdam (Yangtzehaven, Maasvlakte, The Netherlands): A geological and palaeoenvironmental case study for local mapping of Mesolithic lowland landscapes." *Quat. Int.* 367 (May): 4–31. https://doi.org/10.1016/j.quaint.2014.11.056.

White, D. J., and M. D. Bolton. 2004. "Displacement and strain paths during plane-strain model pile installation in sand." *Géotechnique* 54 (6): 375–397. https://doi.org/10.1680/geot.2004.54.6.375.

© ASCE 04024043-12 J. Geotech. Geoenviron. Eng.

J. Geotech. Geoenviron. Eng., 2024, 150(6): 04024043